

WiFi 7 with Different Multi-Link Channel Access Schemes: Modeling, Fairness and Optimization

Jie Zhang, Qingyu Tan, Yayu Gao, *Member, IEEE*, Xinghua Sun, *Member, IEEE*, Wen Zhan, *Member, IEEE*

Abstract—Multi-link operation is regarded as a crucial feature in the upcoming WiFi 7 networks, which allows a single multi-link device (MLD) to make concurrent data transmissions over multiple links. To facilitate synchronous multi-link channel access, IEEE 802.11 Task Group BE has proposed various channel access schemes, such as Longest Backoff (LB) access and Shortest Backoff (SB) access. However, the coexisting performance of WiFi 7 networks with multiple channel access schemes remains largely unexplored. In this paper, we develop an analytical model to evaluate the data rate and mean access delay performance of a multi-link WiFi 7 network with two types of devices adopting LB and SB, respectively, each employing different initial backoff window sizes. The ratio of device data rates between LB-MLDs and SB-MLDs is inversely correlated with the number of links, and the ratio of their initial backoff window sizes, indicating potential unfairness if the backoff parameters are not appropriately chosen. The optimal initial backoff window sizes to maximize the network sum rate and minimize the mean access delay under a given data rate ratio are further derived and verified by simulation results. The maximum network sum rate scales with the number of links, and is independent of the target fairness requirement or number of devices. Conversely, the minimum mean access delay for each type of devices, is strongly influenced by the target fairness requirement, and shows a linear increase with the network size.

Index Terms—IEEE 802.11be, WiFi 7, multi-link operation, optimization.

I. INTRODUCTION

THE brand new WiFi 7, which is based on the IEEE 802.11be amendment, has attracted significant attention from both academia and industry due to its potential in supporting the emerging ultra-high throughput and stringent low-latency applications, such as augmented reality (AR) and online gaming [1]. Specifically, WiFi 7 will expand its bandwidth over a broader and noncontinuous frequency bands

Manuscript received August 14, 2023; revised February 1, 2024; accepted May 6, 2024. The associate editor coordinating the review of this paper and approving it for publication was M. Levorato.

This paper was presented in part at the IEEE International Conference on Communications, Seoul, May 2022.

The work of Y. Gao was supported by Hubei Key Research and Development Program (Grant No. 2023EHA009). The work of X. Sun was supported by Shenzhen Science and Technology Program (Grant No. ZDSYS20210623091807023). The work of W. Zhan was supported in part by Shenzhen Science and Technology Program (No. RCBS20210706092408010) and Open Fund of State Key Laboratory of Satellite Navigation System and Equipment Technology (No. CEPNT-2021KF-04).

J. Zhang, Q. Tan, and Y. Gao are with the School of Electronic Information and Communications, Huazhong University of Science and Technology, Wuhan 430074, P. R. China (e-mail: {jzhang_eic, qingyutan, yayu-gao}@hust.edu.cn).

X. Sun and W. Zhan are with the School of Electronics and Communication Engineering, Shenzhen Campus of Sun Yat-sen University, No. 66. Gongchang Road, Guangming District, Shenzhen, Guangdong 518107, P. R. China (e-mail: {sunxinghua, zhanw6}@mail.sysu.edu.cn).

across 2.4 GHz, 5 GHz and 6 GHz. To maintain efficient utilization among all available spectrum resources, multi-link operation (MLO), which allows concurrent data transmissions on multiple links, is considered as a revolutionary feature in WiFi 7 [2].

A. From Single-Link to Multi-Link

A multi-link device (MLD) has multiple wireless interfaces, corresponding to multiple links under different frequency bands. For an MLD capable of simultaneous transmission and reception (STR) over multiple air interfaces, each interface adopts its own channel access parameters, and can transmit or receive packets independently, known as the asynchronous transmission mode. However, due to in-device power leakage, some devices cannot receive packets on an interface while there are ongoing transmissions on other interfaces, known as the non-STR mode. To address this issue, IEEE 802.11 Task Group BE (TGbe) defines the synchronous transmission mode, where a non-STR MLD can only transmit synchronously on the multiple interfaces.

Legacy single-link WiFi devices operate the distributed coordination function (DCF) according to IEEE 802.11 specifications for channel access control. The basic idea is that with carrier sense multiple access (CSMA), each device would transmit packet only if the channel is sensed idle. Upon transmission failure, the device performs backoff, where a counter is decreased at each idle slot and starts a new transmission once it becomes zero. The value of the counter is randomly selected from $\{0, 1, \dots, W_i - 1\}$, where $W_i = W \cdot 2^i$, $i = 0, 1, \dots, K$. Here, W represents the initial backoff window size, i denotes the backoff stage, which begins at 0 and increments by 1 following each transmission failure until the cutoff phase K is reached.

With MLO, each link of an MLD independently performs the backoff procedure, the likelihood of backoff counters on the multiple links expiring simultaneously is relatively low. To enable the synchronous access mode for non-STR MLDs, TGbe has explored various synchronous channel access schemes, including Longest Backoff (LB) and Shortest Backoff (SB) [3]–[6]. Specifically, LB mandates that an MLD can transmit only when the backoff counters on all links reach zero, whereas SB allows an MLD to transmit when any of the backoff counters reaches zero. The current IEEE 802.11be standard does not specify any particular channel access schemes for non-STR MLDs [7], allowing WiFi vendors the flexibility to customize their implementations and utilize various multi-link channel access schemes in real-world

scenarios, which may result in severe unfairness and malicious resource competition. It is therefore crucial to investigate the effects of different channel access schemes on each other's performance, and further optimize the network performance of an IEEE 802.11be WiFi 7 network with MLDs adopting different channel access schemes.

B. Related Works

A few research studies have been conducted on the performance analysis of the newly-introduced MLO from the perspective of simulations [8]–[11], where it was observed that both data rate and latency performance in STR and non-STR cases can be significantly boosted with MLO. Analytical models were developed based on extensions of the well-known Bianchi model [12] to address a range of multi-link network scenarios, including double-link networks with synchronous access schemes including LB and SB [13], multi-link channel access with automatic repeat request [14], single-link devices and MLDs coexisting networks [15], and unsaturated double-link networks [16]. Based on the model, performance evaluation under given system parameter configuration was conducted including data rate [13]–[15] and delay [16] performance.

In addition to evaluating performance, another crucial aspect that needs attention is the performance optimization of multi-link WiFi 7 networks through the selection of system parameters. The analytical models in [13]–[16] jointly solved a series of equations for deriving the key metrics, such as the successful transmission probability and throughput. Although the development has been substantial, the non-explicit forms of the solutions make it hard for obtaining the optimal system parameter configuration and exploring the performance limit of the multi-link WiFi 7 networks.

The pivotal factor in addressing the performance optimization issue is the modeling approach. In [17], a comprehensive analytical framework was proposed for single-link IEEE 802.11 DCF networks, which examined the dynamics of Head-of-Line (HOL) packets through a discrete-time Markov renewal process. Fundamental performance limits, such as the maximum network throughput and the corresponding optimal system parameters, were obtained. The analysis was further generalized to heterogeneous single-link WiFi networks [18], [19], LTE/5G and WiFi coexisting networks in unlicensed spectrum [20] and multi-link Aloha networks [21]. In this paper, we will extend this model to explore the performance limit of multi-link WiFi 7 networks as well as the way to achieve this limit.

C. Contributions and Main Results

Although in [13], both the Longest Backoff and Shortest Backoff were individually modeled and analyzed, the coexistence of multiple channel access schemes in a single multi-link WiFi 7 network has rarely been considered in the literature. None of the aforementioned models is directly applicable to a WiFi 7 network where MLDs with different channel access schemes coexist. This paper focuses on the modeling, fairness and optimization of a WiFi 7 network with different types

of MLDs, each adopting distinct channel access schemes and backoff parameters. Specifically, the main contributions and key findings of this work can be summarized as follows:

- We propose an analytical model that utilizes the HOL-packet modeling technique introduced in [17] to investigate a saturated M -link WiFi 7 network comprising two types of MLDs, denoted as LB-MLDs and SB-MLDs, which adopt Longest Backoff and Shortest Backoff channel access schemes, respectively. The main emphasis is on characterizing the backoff state, which is very different from the single-link case as it depends on the backoff counters over all the links and varies for different channel access schemes.
- We derive the data rate and mean access delay performance of distinct types of MLDs as explicit functions of system parameters. It is found that the ratio of data rates between LB-MLDs and SB-MLDs is inversely proportional to the ratio of their initial backoff window sizes and the number of links, while the mean access delay of an MLD is inversely proportional to its data rate. The analysis shows if the initial backoff window sizes of LB-MLDs and SB-MLDs are not properly chosen, identical values are adopted for instance, SB-MLDs would achieve much higher data rate than LB-MLDs when the number of links becomes large, leading to severe unfairness.
- We study the fairness-constrained performance optimization, and derive the explicit expressions of the maximum network sum rate, minimum mean access delay, and the corresponding optimal initial backoff window sizes for a given data rate ratio of LB-MLDs to SB-MLDs. The analysis demonstrates that the maximum network sum rate depends solely on the number of links and the transmission parameters, while is independent of the fairness requirement and the number of MLDs. That is, the performance limit of multi-link WiFi 7 networks remains the same regardless of whether there exist multiple different channel access schemes. In order to maximize the network sum rate and minimize the mean access delay while maintaining the target ratio, it is necessary to jointly optimize the initial backoff window sizes of LB-MLDs and SB-MLDs based on factors such as the target ratio, the number of links, the number of LB-MLDs and SB-MLDs, and the transmission parameters.

D. Outline

The remaining sections are outlined as follows. Section II proposes the analytical model for the multi-link WiFi 7 networks, based on which Section III evaluates the data rate and mean access delay. The fairness-constrained network optimization is further studied in Section IV. Following that, Section V presents the simulation results. Finally, Section VI presents concluding remarks.

II. SYSTEM MODEL AND PRELIMINARY ANALYSIS

As Fig. 1 illustrates, consider an M -link WiFi 7 network with two types of MLDs, denoted as Type $\phi = LB, SB$, where $n^{(LB)}$ MLDs adopt Longest Backoff access while

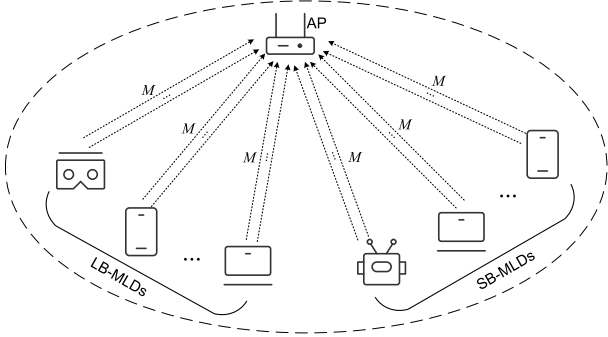


Fig. 1: A WiFi 7 network with LB-MLDs and SB-MLDs.

$n^{(SB)}$ MLDs adopt Shortest Backoff access, all transmitting to a common WiFi 7 access point over the same M links. The MLDs operate in the non-STR mode with synchronous transmissions. We consider a saturated network where each MLD is constantly equipped with packets awaiting transmission. Upon accessing the channel, an MLD concurrently transmits one packet on each of the M links. As devices perform the DCF protocol with different channel access schemes, we assume that MLDs of Type $\phi = LB, SB$ have distinct initial backoff window sizes $W^{(\phi)}$, while sharing the same cutoff phase K .

Graphic illustration of LB and SB is presented in Fig. 2 with $M = 2$. The following conditions apply:

- 1) Each LB-MLD will send the packet if and only if the channel is sensed as idle and all backoff counters on all links have reached zero;
- 2) Each SB-MLD will send the packet if and only if the channel is sensed as idle and at least one of the backoff counters has reached zero.

It is worth noting that the traditional single-link channel access scheme utilized by DCF can be considered as a special scenario where $M = 1$.

Assume that all the MLDs can hear each other, hence subject to strong interference from the others. We adopt the classical collision model, which assumes that if multiple MLDs attempt to transmit their packets on a link simultaneously, a collision will occur, resulting in the failure to decode any of the transmitted packets. Consider no decoding errors due to noise, and a successful transmission occurs when there are no other simultaneous transmissions on the same link.

A. Modeling: An HOL Packet Approach

This paper extends the HOL packet model in [17] to a WiFi 7 network with M individual links. Due to the adoption of synchronous access scheme, the state of HOL packets across all links within the same MLD remains consistent at all times. For instance, as illustrated in Fig. 2, when the SB-MLD accesses the channel, it synchronously transmits on both links, resulting in the successful transmission of packets on both links. In contrast, when both the LB-MLD and SB-MLD access the channel simultaneously, packets on both links of each device collide. Particularly, the probability of successful transmission for each HOL packet on each link of each device is identical, as they either succeed together or collide together.

As a result, we can narrow down to the modeling of the behavior of HOL packets on a specific link, which can be applied to all the other links.

To model the behavior of HOL packets in an MLD of Type $\phi = LB, SB$, we establish a discrete-time Markov renewal process $(\mathbf{X}^{(\phi)}, \mathbf{V}^{(\phi)}) = \{(X_j^{(\phi)}, V_j^{(\phi)})\}, j = 0, 1, \dots\}$. At the j th transition, the state of a tagged HOL packet is represented by $X_j^{(\phi)}$, and $V_j^{(\phi)}$ indicates the epoch of this transition. As illustrated in Fig. 3, the states of an HOL packet can be grouped into three distinct classifications: 1) backoff (State $R_i, i = 0, 1, \dots, K$), 2) collision (State $F_i, i = 0, 1, \dots, K$) and 3) successful transmission (State T).

The limiting probabilities of the Markov renewal process $(\mathbf{X}^{(\phi)}, \mathbf{V}^{(\phi)})$ can be obtained as

$$\tilde{\pi}_j^{(\phi)} = \frac{\pi_j^{(\phi)} \tau_j^{(\phi)}}{\sum_{i \in Q} \pi_i^{(\phi)} \tau_i^{(\phi)}}, \quad (1)$$

where $\phi = LB, SB, j \in Q, Q = \{T, F_0, F_1, \dots, F_K, R_0, R_1, \dots, R_K\}$ denotes the state space of $\mathbf{X}^{(\phi)}$, $\{\pi_j^{(\phi)}\}$ is the steady-state probability distribution of the embedded Markov chain, and $\{\tau_j^{(\phi)}\}$ is the mean holding time of each state.

The probabilities $\{\pi_j^{(\phi)}\}$ can be obtained as

$$\pi_{R_i}^{(\phi)} = \begin{cases} (1-p)^i \pi_T^{(\phi)} & i = 0, 1, \dots, K-1 \\ \frac{(1-p)^K}{p} \pi_T^{(\phi)} & i = K \end{cases} \quad (2)$$

and

$$\pi_{F_i}^{(\phi)} = \pi_{R_i}^{(\phi)} \cdot (1-p), \quad i = 0, 1, \dots, K, \quad (3)$$

where p represents the steady-state probability of successfully transmitting HOL packets when the link is sensed as idle.

As shown in Fig. 2, the holding time $\tau_T^{(LB)} = \tau_T^{(SB)} = \tau_T$ (in the unit of time slots) in State T and the holding time $\tau_F^{(LB)} = \tau_F^{(SB)} = \tau_F$ (in the unit of time slots) in States $F_i, i = 0, 1, \dots, K$, are dependent on the system parameters selected by the MLDs, which can be written as

$$\tau_T = \frac{(L_P + L_{MH})/R + \text{SIFS} + L_{ACK}/R_B + \text{DIFS} + T_{PH}}{\sigma} \quad (4)$$

and

$$\tau_F = \frac{(L_P + L_{MH})/R + \text{DIFS} + T_{PH}}{\sigma}, \quad (5)$$

respectively, where L_P, L_{MH} , and L_{ACK} denote the lengths of the packet payload, MAC header, and ACK, respectively, all in the unit of bits, R and R_B denote the transmission rate and basic rate, respectively, all in the unit of Mbps, T_{PH} and σ denote the lengths of the PHY preamble and a time slot, all in the unit of μs , SIFS and DIFS are also in the unit of μs .

In contrast, the mean holding time $\tau_{R_i}^{(\phi)}$ (in the unit of time slots) of an HOL packet in States $R_i, i = 0, 1, \dots, K$ for an MLD of Type ϕ , significantly relies on the channel access scheme and backoff parameters the MLD adopts. Similar to the scenario with a single link, in an MLD of Type $\phi = LB, SB$, HOL packets on the M links enter State R_i simultaneously, and initialize their individual backoff counters by randomly selecting a value from $\{0, 1, \dots, W_i^{(\phi)} - 1\}$, where $W_i^{(\phi)} = W^{(\phi)} \cdot 2^i$ represents the backoff window size in backoff stage $i = 0, 1, \dots, K$. These HOL packets then count down the

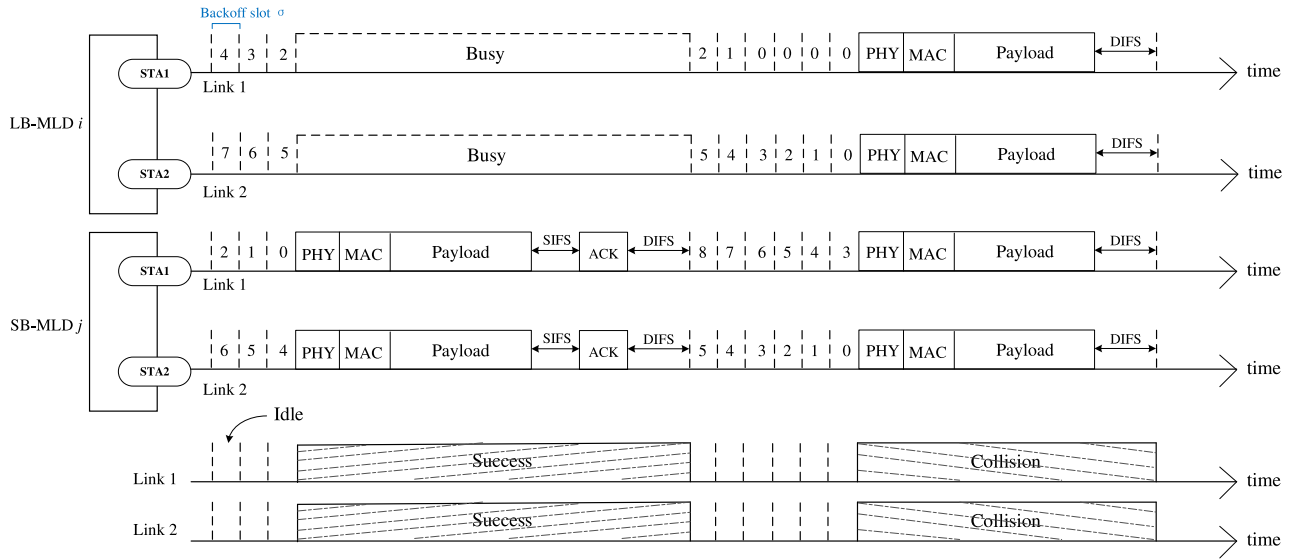


Fig. 2: Packet transmissions of LB-MLDs and SB-MLDs in a two-link WiFi 7 network.

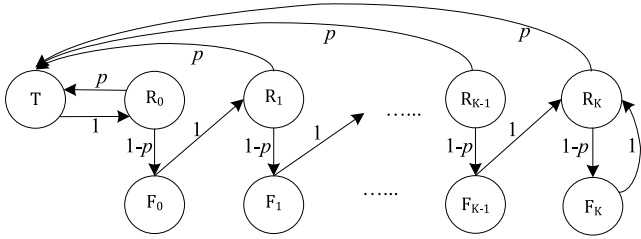


Fig. 3: Embedded Markov chain $\{X_j^{(\phi)}\}$ of each HOL packet's state transition process for an MLD of Type $\phi = LB, SB$.

backoff counters at each idle slot. Nevertheless, in contrast to the situation with a single link, the HOL packet on a specific link could remain in State R_i even after its individual backoff counter is declined to zero. Specifically, HOL packets on all the M links of the same MLD simultaneously transition out of State R_i , and attempt to transmit when the *shared backoff counter* of the MLD is decreased to 0 and the channel is sensed to be idle. The *shared backoff counter* refers to the number of idle time slots required for an HOL packet to leave the backoff state R_i , the value of which is closely tied to the type of MLDs. In particular,

- 1) For each LB-MLD, the *shared backoff counter* is the largest one among the individual counters on all the M links;
- 2) For each SB-MLD, the *shared backoff counter* is the smallest one among the individual counters on all the M links.

The steady-state conditional transmission probability, denoted as $r_i^{(\phi)}$, for a State- R_i HOL packet to initiate a transmission when the channel is idle, can be approximated as

$$r_i^{(LB)} \approx \frac{1}{\frac{MW_i^{(LB)}}{M+1} + \frac{1}{2}} \quad (6)$$

and

$$r_i^{(SB)} \approx \frac{1}{\frac{W_i^{(SB)}}{M+1} + \frac{1}{2}}, \quad (7)$$

for LB-MLDs and SB-MLDs, respectively, when $\{W^{(\phi)}\}$ are sufficiently considerable. Appendix A presents the derivation of (6) and (7).

In the beginning of each slot, an MLD of Type $\phi = LB, SB$ with a State- R_i HOL packet would sense the channel, and transmits with probability $r_i^{(\phi)}$ if the channel is idle. Therefore, the mean holding time $\tau_{R_i}^{(\phi)}$ in State R_i can be written as

$$\tau_{R_i}^{(\phi)} = \frac{1}{\alpha_{R_i}^{(\phi)} r_i^{(\phi)}}, \quad (8)$$

where $\alpha_{R_i}^{(\phi)}$ denotes the conditional probability that an MLD of Type ϕ with State- R_i HOL packets senses the channel idle, $\phi = LB, SB$. As shown in Appendix B, $\alpha_{R_i}^{(\phi)}$ can be derived as

$$\alpha_{R_i}^{(\phi)} = \frac{\alpha}{1 - \tilde{\pi}_T^{(\phi)} \left(1 + \frac{\tau_F(1-p)}{\tau_T p}\right)}, \quad (9)$$

where α is the steady-state probability that the channel is idle, which can be obtained as

$$\alpha = \frac{1}{1 + \tau_F - \tau_T p - (\tau_T - \tau_F)p \ln p}, \quad (10)$$

by following a similar derivation in [17].

By combining (1)-(3) and (8), the steady-state probability of an HOL packet of Type $\phi = LB, SB$ to be in State T can be obtained as

$$\tilde{\pi}_T^{(\phi)} = \frac{1}{1 + \frac{\tau_F}{\tau_T} \frac{1-p}{p} + \frac{1}{\tau_T} \left(\sum_{i=0}^{K-1} \frac{(1-p)^i}{\alpha_{R_i}^{(\phi)} r_i^{(\phi)}} + \frac{(1-p)^K}{p \alpha_{R_K}^{(\phi)} r_K^{(\phi)}} \right)}. \quad (11)$$

By substituting (9) into (11), $\tilde{\pi}_T^{(\phi)}$ can be solved as

$$\tilde{\pi}_T^{(\phi)} = \frac{\alpha \tau_T}{\sum_{i=0}^{K-1} \frac{(1-p)^i}{r_i^{(\phi)}} + \frac{(1-p)^K}{p r_K^{(\phi)}}}. \quad (12)$$

It is worth mentioning that $\tilde{\pi}_T^{(\phi)}$ is the service rate of the queue for each MLD on a single link, as the queue can have a successful output only when the HOL packet stays in State T.

By combining (6)-(7) and (12), $\tilde{\pi}_T^{(LB)}$ and $\tilde{\pi}_T^{(SB)}$ can further be approximately obtained as

$$\tilde{\pi}_T^{(LB)} \approx \frac{(M+1)\alpha\tau_T}{MW^{(LB)}} \cdot \frac{p(2p-1)}{p-2^K(1-p)^{K+1}} \quad (13)$$

and

$$\tilde{\pi}_T^{(SB)} \approx \frac{(M+1)\alpha\tau_T}{W^{(SB)}} \cdot \frac{p(2p-1)}{p-2^K(1-p)^{K+1}}, \quad (14)$$

respectively.

B. Steady-state Operating Point

The analysis above reveals the significant impact of the steady-state probability of successfully transmitting HOL packets when the channel is idle, denoted as p , on the performance of multi-link WiFi 7 networks. This subsection will further characterize the steady-state operating point of saturated multi-link WiFi 7 networks by establishing a fixed-point equation for p .

When the network is saturated, the successful transmission of an HOL packet from a specific MLD of Type ϕ depends on the absence of transmission requests from the other $n^{(\phi)} - 1$ MLDs of the same type and all the $n^{(\psi)}$ MLDs of Type $\psi \neq \phi$. Therefore, the steady-state probability of successfully transmitting HOL packets when the channel is idle, is given by

$$p = (\Pr\{\text{MLD of Type } \phi \text{ do not transmit} \\ \mid \text{channel is idle}\})^{n^{(\phi)}-1} \cdot (\Pr\{\text{MLD of Type } \psi \neq \phi \\ \text{do not transmit} \mid \text{channel is idle}\})^{n^{(\psi)}}. \quad (15)$$

When the number of MLDs in each type is large, (15) can be approximated as

$$p \approx \prod_{\phi=LB,SB} (\Pr\{\text{MLD of Type } \phi \text{ do not transmit} \\ \mid \text{channel is idle}\})^{n^{(\phi)}} \\ = \prod_{\phi=LB,SB} \left(1 - \frac{\tilde{\pi}_T^{(\phi)}}{\tau_T \alpha p}\right)^{n^{(\phi)}}. \quad (16)$$

The derivation of (16) is provided in detail in Appendix C.

By combining (12) and (16), we have

$$p = \prod_{\phi=LB,SB} \left(1 - \frac{1}{\sum_{i=0}^{K-1} \frac{p(1-p)^i}{r_i^{(\phi)}} + \frac{(1-p)^K}{r_K^{(\phi)}}}\right)^{n^{(\phi)}}. \quad (17)$$

By applying $(1-y)^n \approx e^{-ny}$ for large n and small y , and combining with (6)-(7), (17) can be further written as

$$p = \exp \left\{ \frac{-\left(\frac{n^{(LB)}}{MW^{(LB)}} + \frac{n^{(SB)}}{W^{(SB)}}\right) (M+1)(2p-1)}{p-2^K(1-p)^{K+1}} \right\}. \quad (18)$$

The non-zero root of the fixed-point equation of p in (18) is referred to as the network steady-state operating point p_A . (18) shows that p_A is ascertained by the number of links M , the numbers of MLDs $\{n^{(\phi)}\}$, the initial backoff window sizes $\{W^{(\phi)}\}$, and the cutoff phase K , of the two types of MLDs $\phi = LB, SB$.

III. DATA RATE AND MEAN ACCESS DELAY ANALYSIS

This section further characterizes the data rate and mean access delay performance of saturated multi-link WiFi 7 networks at the steady-state operating point p_A , utilizing the analytical model presented in Section II.

A. Data Rate

Let us first investigate the data rate performance, which refers to the quantity of information bits successfully transmitted per second. As shown in Fig. 2, the data rate $D^{(\phi)}$ of each MLD of Type $\phi = LB, SB$ depends on 1) the number of links M , 2) the service rate $\tilde{\pi}_T^{(\phi)}$ on each link, 3) the proportion of time dedicated to transmitting packet payload in a successful transmission and 4) the transmission rate R , and can be expressed as

$$D^{(\phi)} = M \cdot \tilde{\pi}_T^{(\phi)} \cdot \frac{L_P}{\sigma R} \cdot R = M \tilde{\pi}_T^{(\phi)} \cdot \frac{L_P}{\sigma \tau_T}. \quad (19)$$

By substituting (13) and (14) into (19), the device data rates can be further derived as

$$D^{(LB)} = \frac{(M+1)\alpha L_P}{\sigma W^{(LB)}} \cdot \frac{p_A(2p_A-1)}{p_A-2^K(1-p_A)^{K+1}} \quad (20)$$

and

$$D^{(SB)} = \frac{M(M+1)\alpha L_P}{\sigma W^{(SB)}} \cdot \frac{p_A(2p_A-1)}{p_A-2^K(1-p_A)^{K+1}}, \quad (21)$$

for LB-MLDs and SB-MLDs, respectively.

According to (20) and (21), the ratio of data rates between LB-MLDs and SB-MLDs can then be obtained as

$$\frac{D^{(LB)}}{D^{(SB)}} = \frac{W^{(SB)}}{MW^{(LB)}}. \quad (22)$$

Note that it has been found in [19] that for single-link WiFi networks with groups of devices adopting distinct initial backoff window sizes, the ratio of device throughput is inversely correlated with the ratio of their initial backoff window sizes. For multi-link WiFi 7 networks with LB-MLDs and SB-MLDs, it is captivating to observe that the ratio of data rates $\frac{D^{(LB)}}{D^{(SB)}}$ is not only inversely proportional to that of their initial backoff window sizes, but the number of links M as well. This implies that when LB-MLDs and SB-MLDs adopt equal initial backoff window sizes, the data rate of LB-MLDs is only $\frac{1}{M}$ of that of SB-MLDs, resulting in significant unfairness, particularly when there is a large number of links M .

The reason lies in the design of these two channel access schemes. In particular, LB-MLDs can access the channel only if all the backoff counters of the M links reach zero while SB-MLDs can access the channel if any of the backoff counters reaches zero. Consequently, as the number of links M increases, the average time of waiting to request a transmission

for LB-MLDs becomes longer compared to that for SB-MLDs, leading to a lower chance for making transmission attempts and therefore a lower data rate.

The total data rates of all MLDs in the network, denoted by the network sum rate \hat{D} , can be expressed as

$$\begin{aligned} \hat{D} &= \sum_{\phi=LB,SB} n^{(\phi)} D^{(\phi)} \\ &= \frac{-ML_P p_A \ln p_A}{\sigma(1 + \tau_F - \tau_F p_A - (\tau_T - \tau_F) p_A \ln p_A)}, \end{aligned} \quad (23)$$

by combining (10), (18), (20) and (21). As indicated by (23), the network sum rate \hat{D} is governed by the network's steady-state operating point p_A , which is influenced by the backoff parameters of the MLDs.

B. Mean Access Delay

This subsection derives the mean access delay of HOL packets of Type $\phi = LB, SB$, and explore how different channel access schemes affect the mean access delay performance in multi-link WiFi 7 networks.

Denote $Y_i^{(\phi)}$ as the holding time in State R_i , and $AD_i^{(\phi)}$ as the duration from the start of State R_i until the completion of service for an HOL packet of Type $\phi = LB, SB$. According to Fig. 3, we have

$$AD_i^{(\phi)} = \begin{cases} Y_i^{(\phi)} + \tau_T & \text{with probability } p \\ Y_i^{(\phi)} + \tau_F + AD_{i+1}^{(\phi)} & \text{with probability } 1-p, \end{cases} \quad (24)$$

$i = 0, 1, \dots, K-1$, and

$$AD_K^{(\phi)} = \begin{cases} Y_K^{(\phi)} + \tau_T & \text{with probability } p \\ Y_K^{(\phi)} + \tau_F + AD_K^{(\phi)} & \text{with probability } 1-p. \end{cases} \quad (25)$$

The probability generating functions of $AD_i^{(\phi)}$, denoted as $G_{AD_i^{(\phi)}}(z)$, $\phi = LB, SB$, can be derived from (24) and (25) as

$$G_{AD_i^{(\phi)}}(z) = \begin{cases} pz^{\tau_T} G_{Y_i^{(\phi)}}(z) + (1-p)z^{\tau_F} \cdot \\ G_{Y_i^{(\phi)}}(z) G_{AD_{i+1}^{(\phi)}}(z) & i=0, 1, \dots, K-1, \\ pz^{\tau_T} G_{Y_K^{(\phi)}}(z) + (1-p)z^{\tau_F} \cdot \\ G_{Y_K^{(\phi)}}(z) G_{AD_K^{(\phi)}}(z) & i=K. \end{cases} \quad (26)$$

Note that $AD_0^{(\phi)}$ is the service time of HOL packets, i.e., the access delay, in MLDs of Type ϕ . According to (26), we have

$$\begin{aligned} G'_{AD_0^{(\phi)}}(1) &= \tau_T + \frac{1-p}{p} \tau_F + \sum_{i=0}^{K-1} (1-p)^i G'_{Y_i^{(\phi)}}(1) \\ &\quad + \frac{(1-p)^K}{p} G'_{Y_K^{(\phi)}}(1), \end{aligned} \quad (27)$$

$\phi = LB, SB$, where $G'_{Y_i^{(\phi)}}(1)$ is the mean holding time of an HOL packet in State R_i , i.e., $\tau_{R_i}^{(\phi)}$, which has been given in (8).

By combining (6)-(9) with (27), the mean access delay $E[AD_0^{(\phi)}] = G'_{AD_0^{(\phi)}}(1)$ (in the unit of time slots) of an MLD of Type $\phi = LB, SB$ can be obtained as

$$E[AD_0^{(LB)}] \approx \frac{MW^{(LB)}}{\alpha(M+1)} \cdot \frac{p_A - 2^K(1-p_A)^{K+1}}{p_A(2p_A - 1)} \quad (28)$$

and

$$E[AD_0^{(SB)}] \approx \frac{W^{(SB)}}{\alpha(M+1)} \cdot \frac{p_A - 2^K(1-p_A)^{K+1}}{p_A(2p_A - 1)}, \quad (29)$$

respectively.

A closer look at (28) and (29) shows that for a saturated network, the mean access delay $E[AD_0^{(\phi)}]$ of each MLD of Type $\phi = LB, SB$ is negatively associated with its data rate $D^{(\phi)}$, i.e.,

$$E[AD_0^{(\phi)}] = \frac{ML_P}{\sigma D^{(\phi)}}. \quad (30)$$

Furthermore, the ratio of the mean access delay of LB-MLDs to that of SB-MLDs can be obtained as

$$\frac{E[AD_0^{(LB)}]}{E[AD_0^{(SB)}]} = \frac{MW^{(LB)}}{W^{(SB)}}, \quad (31)$$

which is proportional to both the ratio of their initial backoff window sizes and the number of links M .

We can conclude that when LB-MLDs and SB-MLDs coexist in a multi-link WiFi 7 network, the ratio of their data rates and mean access delays are highly influenced by their initial backoff window sizes $\{W^{(\phi)}\}$, and the number of links M . As SB-MLDs are more aggressive compared to LB-MLDs when accessing the channel, severe unfairness can occur without proper selection of backoff parameters.

IV. FAIRNESS-CONSTRAINED PERFORMANCE OPTIMIZATION

Section III highlighted the significant influence of the parameter setting of LB-MLDs and SB-MLDs on the fairness and overall network performance of the coexisting networks. In this section, we will further investigate the optimization of the network sum rate and mean access delay performance while considering specific fairness requirements.

Let γ be the target ratio of device data rates between LB-MLDs and SB-MLDs. By adjusting the initial backoff window sizes $\{W^{(\phi)}\}$ for MLDs of Type $\phi = LB, SB$, we can determine the maximum network sum rate \hat{D}_{\max} for a given γ , which can be formulated as

$$\begin{aligned} \hat{D}_{\max} &= \max_{W^{(LB)}, W^{(SB)}} \hat{D}, \\ \text{s.t. } \frac{D^{(LB)}}{D^{(SB)}} &= \gamma. \end{aligned} \quad (32)$$

The solution to the optimization problem stated above, i.e., the maximum network sum rate \hat{D}_{\max} and the corresponding optimal initial backoff window sizes $\{W_m^{(\phi)}\}$ for MLDs of Type $\phi = LB, SB$, is presented in the following theorem.

Theorem 1. *The maximum network sum rate \hat{D}_{\max} , as defined in (32), is given by*

$$\hat{D}_{\max} = \frac{-ML_P \cdot \mathbb{W}_0 \left(-\frac{1}{e(1+1/\tau_F)} \right)}{\sigma \left(\tau_F - (\tau_T - \tau_F) \mathbb{W}_0 \left(-\frac{1}{e(1+1/\tau_F)} \right) \right)}, \quad (33)$$

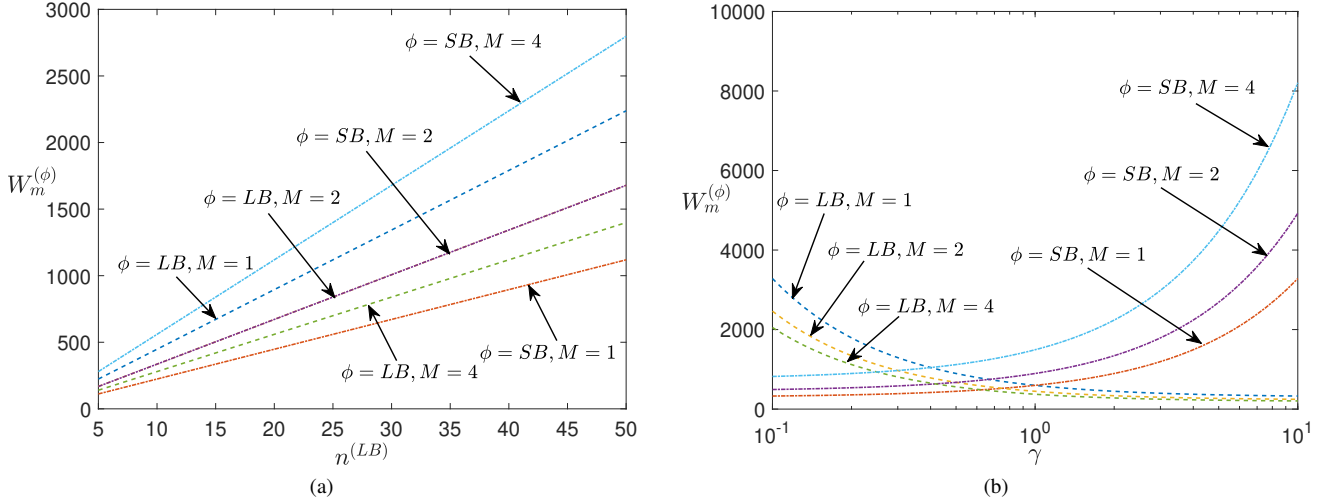


Fig. 4: Optimal initial backoff window size $W_m^{(\phi)}$, $\phi = LB, SB$. (a) $W_m^{(\phi)}$ versus the number of LB-MLDs $n^{(LB)}$ with $n^{(SB)} = n^{(LB)}$. $\gamma = 0.5$. (b) $W_m^{(\phi)}$ versus the target data rate ratio γ . $n^{(LB)} = n^{(SB)} = 20$.

where $\mathbb{W}_0(\cdot)$ denotes the principal branch of the Lambert W function [22]. To achieve \hat{D}_{\max} , the initial backoff window sizes should be set as

$$W^{(LB)} = W_m^{(LB)} = \left(\frac{1}{M} + 1 \right) \left(n^{(LB)} + \frac{1}{\gamma} n^{(SB)} \right) \cdot \frac{1 - 2p_A^*}{(p_A^* - 2^K(1 - p_A^*)^{K+1}) \ln p_A^*} \quad (34)$$

and

$$W^{(SB)} = W_m^{(SB)} = (M + 1)(\gamma n^{(LB)} + n^{(SB)}) \cdot \frac{1 - 2p_A^*}{(p_A^* - 2^K(1 - p_A^*)^{K+1}) \ln p_A^*}, \quad (35)$$

where p_A^* is the optimal network steady-state operating point, and is given by

$$p_A^* = -(1 + 1/\tau_F) \mathbb{W}_0 \left(-\frac{1}{e(1 + 1/\tau_F)} \right). \quad (36)$$

Proof. It can be seen from (23) that the network sum rate \hat{D} is a function of the network steady-state operating point p_A . By taking the derivative of \hat{D} , the maximum network sum rate \hat{D}_{\max} can be obtained as (33), which is achieved when $p_A = p_A^*$ as given in (36), by following a similar derivation in [17].

By combining (22) and (32), we have

$$\frac{W^{(SB)}}{W^{(LB)}} = M \cdot \gamma. \quad (37)$$

According to (18), the optimal initial backoff window sizes need to satisfy that

$$\frac{n^{(LB)}}{M W^{(LB)}} + \frac{n^{(SB)}}{W^{(SB)}} = \frac{(p_A^* - 2^K(1 - p_A^*)^{K+1}) \ln p_A^*}{(M + 1)(1 - 2p_A^*)}. \quad (38)$$

(34) and (35) can be obtained by combining (37) and (38). \square

Theorem 1 reveals that the maximum network sum rate \hat{D}_{\max} of multi-link WiFi 7 network with SB/LB access schemes depends solely on the time slot length σ , the payload

TABLE I: Basic Setting of Network Parameters [7]

Parameter	Value
Time slot length σ	9 μ s
PHY preamble length T_{PH}	20 μ s
SIFS	16 μ s
DIFS	34 μ s
ACK length L_{ACK}	112 bits
Payload length L_P	2^{17} bits
MAC header length L_{MH}	288 bits
Link bandwidth	20 MHz
Basic rate R_B	24 Mbps
Transmission rate R	114.7 Mbps
Cutoff phase K	6

length L_P , the number of links M , and the holding times in successful transmission and collision, τ_T and τ_F , which are governed by transmission parameters. \hat{D}_{\max} is independent of the target ratio of device data rates γ , or the numbers of LB-MLDs and SB-MLDs, $n^{(LB)}$ and $n^{(SB)}$. It indicates that the fairness requirement between LB-MLDs and SB-MLDs, or whether there exist multiple different channel access schemes or a single one, i.e., $n^{(LB)} = 0$ or $n^{(SB)} = 0$, would not affect the limit of network sum rate of a multi-link WiFi 7 network.

In order to maximize the network sum rate while maintaining the target ratio of device data rates, we can clearly see from (34) and (35) that the optimal initial backoff window sizes $W_m^{(LB)}$ and $W_m^{(SB)}$ depend closely on 1) the number of links M , 2) the numbers of devices $\{n^{(\phi)}\}$, $\phi = LB, SB$, and 3) the target ratio of device data rates γ . For illustration, Fig. 4 depicts the optimal initial backoff window sizes $W_m^{(LB)}$ and $W_m^{(SB)}$ of saturated multi-link WiFi 7 networks. This paper adopts system parameters in accordance with the IEEE 802.11be draft standard [7], as presented in TABLE I. With these parameters, (34) and (35) can then be written as

$$W_m^{(LB)} = 7.46 \left(\frac{1}{M} + 1 \right) \left(n^{(LB)} + \frac{1}{\gamma} n^{(SB)} \right) \quad (39)$$

and

$$W_m^{(SB)} = 7.46(M + 1)(\gamma n^{(LB)} + n^{(SB)}), \quad (40)$$

respectively.

As depicted in Fig. 4(a), both $W_m^{(LB)}$ and $W_m^{(SB)}$ exhibit a linear increase in relation to the numbers of MLDs $n^{(LB)}$ and $n^{(SB)}$. Moreover, as the number of links M grows, $W_m^{(LB)}$ decreases while $W_m^{(SB)}$ increases. In Section II, it has been demonstrated that the *shared backoff counter* of an LB-MLD corresponds to the maximum value among the M counters, leading to an increase in its average value with larger M . Consequently, it is advisable to reduce the initial backoff window size for LB-MLDs when M grows. Conversely, an SB-MLD has a *shared backoff counter* that determined by the minimum of all the counters. This results in a decrease in its average value as M increases, consequently leading to an increase in $W_m^{(SB)}$.

Fig. 4(b) further shows that as the target data rate ratio γ increases, the optimal initial backoff window size of SB-MLDs $W_m^{(SB)}$ steadily increases, while that of LB-MLDs $W_m^{(LB)}$ decreases. Intuitively, as γ increases, LB-MLDs are to maintain higher data rate performance, therefore, they should decrease their initial backoff window size so as to increase their chances of accessing the channel, while SB-MLDs should reduce their chances to transmit by enlarging their initial backoff window size.

Let us further consider how to minimize the mean access delays of LB-MLDs and SB-MLDs under the target ratio of device data rates γ , which can be written as

$$\begin{aligned} E[AD_0^{(\phi)}]_{\min} &= \min_{W^{(LB)}, W^{(SB)}} E[AD_0^{(\phi)}], \\ s.t. \quad \frac{D^{(LB)}}{D^{(SB)}} &= \gamma, \end{aligned} \quad (41)$$

$\phi = LB, SB$. Recall that the mean access delay $E[AD_0^{(\phi)}]$ is inversely proportional to the device data rate $D^{(\phi)}$. As the ratio of $D^{(LB)}$ to $D^{(SB)}$ is given, when the network sum rate \hat{D} is maximized, the mean access delay $E[AD_0^{(\phi)}]$ is minimized. Corollary 1 presents the minimum mean access delays of LB-MLDs and SB-MLDs under the target ratio of device data rates γ , i.e., the solution to (41).

Corollary 1. *The minimum mean access delays of LB-MLDs and SB-MLDs and the target ratio of device data rates γ is achieved when the initial backoff window sizes of LB-MLDs and SB-MLDs are set as (34) and (35), respectively. The minimum mean access delays of LB-MLDs and SB-MLDs are given by*

$$\begin{aligned} E \left[AD_0^{(LB)} \right]_{\min} &= (n^{(LB)} + \frac{1}{\gamma} n^{(SB)}) \\ &\cdot \frac{\tau_F - (\tau_T - \tau_F) \mathbb{W}_0 \left(-\frac{1}{e(1+1/\tau_F)} \right)}{-\mathbb{W}_0 \left(-\frac{1}{e(1+1/\tau_F)} \right)} \end{aligned} \quad (42)$$

and

$$\begin{aligned} E \left[AD_0^{(SB)} \right]_{\min} &= (\gamma n^{(LB)} + n^{(SB)}) \\ &\cdot \frac{\tau_F - (\tau_T - \tau_F) \mathbb{W}_0 \left(-\frac{1}{e(1+1/\tau_F)} \right)}{-\mathbb{W}_0 \left(-\frac{1}{e(1+1/\tau_F)} \right)}, \end{aligned} \quad (43)$$

respectively.

We can observe from Corollary 1 that although the maximum network sum rate \hat{D}_{\max} is invariant to the number of MLDs, the minimum mean access delay $E[AD_0^{(\phi)}]_{\min}$ of each MLD inevitably increases linearly as the network size grows. It indicates that if stringent delay constraint is to be satisfied, adaptive admission control schemes need to be included. Consider given mean access delay constraints of LB-MLDs and SB-MLDs, denoted as $C^{(LB)}$ and $C^{(SB)}$, respectively (in the unit of time slots). To ensure that the mean access delays of LB-MLDs and SB-MLDs do not exceed the given constraints, i.e., $E[AD_0^{(\phi)}] \leq C^{(\phi)}$, $\phi = LB, SB$, the numbers of LB-MLDs and SB-MLDs for a saturated IEEE 802.11be WiFi 7 network need to satisfy the following inequality

$$\begin{aligned} (\gamma n^{(LB)} + n^{(SB)}) &\leq \min\{\gamma C^{(LB)}, C^{(SB)}\} \\ &\cdot \frac{-\mathbb{W}_0 \left(-\frac{1}{e(1+1/\tau_F)} \right)}{\tau_F - (\tau_T - \tau_F) \mathbb{W}_0 \left(-\frac{1}{e(1+1/\tau_F)} \right)}, \end{aligned} \quad (44)$$

according to (42) and (43). Once (44) is not satisfied, additional devices should be not admitted to access so as to ensure the delay constraints of LB-MLDs and SB-MLDs are achievable. With the system parameters shown in TABLE I, (44) can then be written as

$$(\gamma n^{(LB)} + n^{(SB)}) \leq 0.0065 \cdot \min\{\gamma C^{(LB)}, C^{(SB)}\}. \quad (45)$$

V. SIMULATION RESULTS

Simulation results are presented in this section to verify the analysis above. A summary of the network parameters for simulations can be found in TABLE I.

A. Fixed Setting

We begin by examining the scenario where MLDs adopt fixed initial backoff window sizes, which is the default configuration in the current IEEE 802.11 standard. The device data rate $D^{(\phi)}$ of MLDs and the network sum rate \hat{D} have been derived in (20), (21) and (23), respectively. Fig. 5 presents the variation in data rate performance for multi-link WiFi 7 networks as the network size changes. The left vertical axis represents the data rate of each device, while the right vertical axis represents the network sum rate. Fig. 5 clearly demonstrates that the network sum rate experiences a rapid deterioration when the number of MLDs in the network becomes large, owing to the escalating contention level. For example, the network sum rate \hat{D} with $M = 4$ drops from 380Mbps to 276Mbps as the number of LB-MLDs and SB-MLDs increases from 5 to 100. Moreover, it shows that LB-MLDs exhibit significantly lower data rates compared to SB-MLDs when both adopt the same initial backoff window size. With $M = 2$, the data rate of LB-MLDs is only a half of that of SB-MLDs, and with $M = 4$, it is only one fourth.

Further observation on Fig.5 reveals that the simulation results exhibit minor deviations from the analytical values, particularly noticeable when $M = 4$. In particular, the simulated data rates of SB-MLDs tend to be higher than

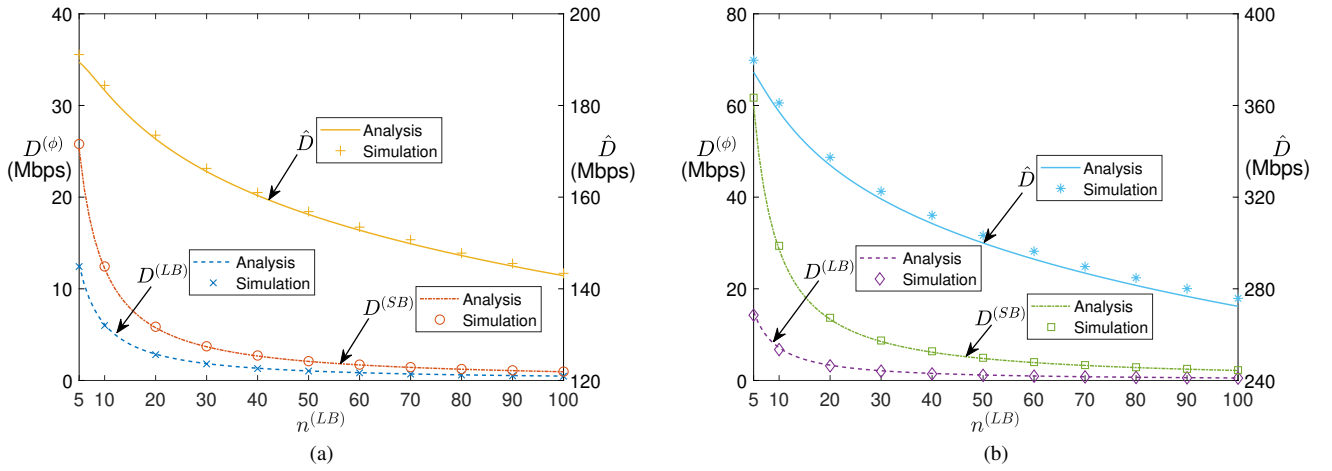


Fig. 5: Device data rate $D^{(\phi)}$, $\phi = LB, SB$, and network sum rate \hat{D} versus the number of LB-MLDs $n^{(LB)}$ in saturated multi-link WiFi 7 networks with fixed initial backoff window sizes. $n^{(SB)} = n^{(LB)}$. $W^{(LB)} = W^{(SB)} = 128$. (a) $M = 2$. (b) $M = 4$.

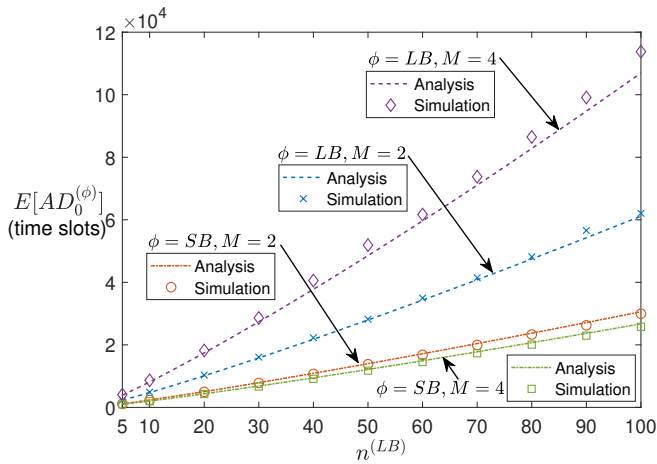


Fig. 6: Mean access delay $E[AD_0^{(\phi)}]$, $\phi = LB, SB$, versus the number of LB-MLDs $n^{(LB)}$ in saturated multi-link WiFi 7 networks with fixed initial backoff window sizes. $n^{(SB)} = n^{(LB)}$. $W^{(LB)} = W^{(SB)} = 128$.

the analytical ones. This divergence can be attributed to the ‘‘capture effect’’ observed under saturated conditions, wherein MLDs experience long backoff duration due to large backoff stages, and once one MLD transmits successfully, it tend to grab the channel for multiple consecutive transmissions. Consequently, the assumption of a time-homogeneous backoff process for each MLD becomes less valid. Since SB-MLDs select the smallest one among M values, they tend to have more chances to transmit and a higher probability to benefit from the capture effect, leading to higher data rates especially when M is large. However, with a significantly large initial backoff window size, the transmission attempts become more randomly distributed over time and the capture effect can be diminished. The following subsection will demonstrate that simulation results align well with analytical results under optimal initial backoff window sizes.

The mean access delays of LB-MLDs and SB-MLDs, given

in (28) and (29), respectively, are verified through simulation results. As shown in Fig. 6, it is evident that the mean access delays of both type of MLDs increase significantly as the number of MLDs increases due to the growing congestion level. However, the mean access delay of SB-MLDs is lower than that of LB-MLDs, owing to the more aggressive channel access of SB-MLDs.

We can conclude from Figs. 5 and 6 that if the initial backoff window sizes are fixed, then the network performance inevitably deteriorates as the network size increases. In the meanwhile, the ratio of data rates and mean access delays of LB-MLDs and SB-MLDs are closely tied to the number of links M , and may lead to severe unfairness when M is large.

B. Optimal Setting

Theorem 1 presented in Section IV reveals that by properly tuning the initial backoff window sizes for LB-MLDs and SB-MLDs using (34) and (35) respectively, the network sum rate can be maximized while the rate fairness being guaranteed. Fig. 7(a) presents the data rate performance with the optimal initial backoff window sizes $\{W_m^{(\phi)}\}$ with the target data rate ratio $\gamma = 1$. We can clearly see from Fig. 7(a) that different from the fixed setting case, the optimal setting achieves the maximum network sum rate \hat{D}_{\max} regardless of network size variations. In the meanwhile, the data rates of LB-MLDs and SB-MLDs are always identical, indicating that the target data rate ratio can always be maintained.

Corollary 1 has shown that the mean access delay is minimized with the optimal initial backoff window sizes. Fig. 7(b) shows that the minimum mean access delay exhibits a linear increase as the number of devices grows. Furthermore, when considering $\gamma = 1$, both LB-MLDs and SB-MLDs achieve an equal mean access delay, as the mean access delay is inversely proportional to the device data rate.

Fig. 8 depicts the variations in device data rates and network sum rate as the target data rate ratio changes. It can be seen that with the optimal setting, we can achieve an arbitrary target

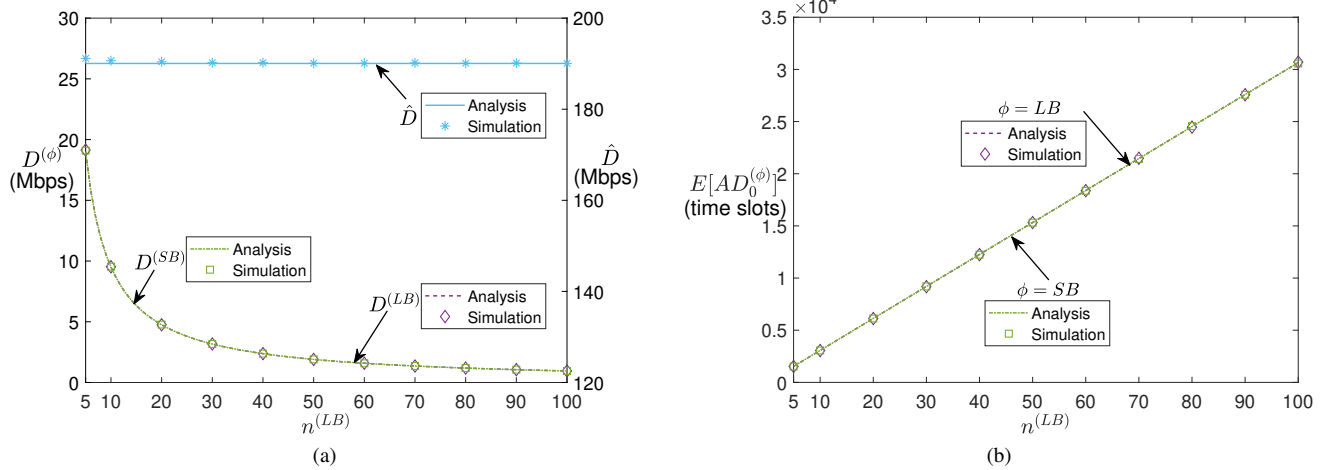


Fig. 7: Device data rate $D^{(\phi)}$, $\phi = LB, SB$, network sum rate \hat{D} and mean access delay $E[AD_0^{(\phi)}]$, $\phi = LB, SB$ versus the number of LB-MLDs $n^{(LB)}$ in saturated multi-link WiFi 7 networks with optimal initial backoff window sizes $\{W_m^{(\phi)}\}$. $n^{(SB)} = n^{(LB)}$. $M = 2$. $\gamma = 1$. (a) Device data rate and network sum rate. (b) Mean access delay.

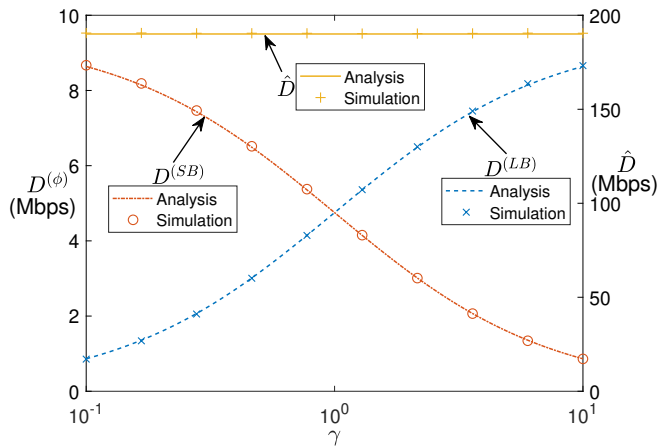


Fig. 8: Device data rate $D^{(\phi)}$, $\phi = LB, SB$, and network sum rate \hat{D} versus the target ratio of the data rate of LB-MLDs to that of SB-MLDs, γ , in saturated multi-link WiFi 7 networks with optimal initial backoff sizes $\{W_m^{(\phi)}\}$. $n^{(LB)} = n^{(SB)} = 20$. $M = 2$.

ratio while maintaining the maximum network sum rate. In practice, the target data rate ratio can be considered as a control knob for the network manager to assign different priorities to distinct device types, depending on the specific requirement of each type of devices.

VI. CONCLUSIONS

This paper evaluates and optimizes the performance of multi-link WiFi 7 networks with coexisting LB-MLDs and SB-MLDs. By deriving the steady-state probability of successful transmission as a function of the backoff parameters, we obtain explicit expressions of data rates and mean access delays for different types of MLDs. The analysis reveals that the data rate ratio between LB-MLDs and SB-MLDs is inversely related to the ratio of their initial backoff window sizes and the number of links. Additionally, the mean access delay of an MLD is

inversely proportional to its data rate. Consequently, when LB-MLDs and SB-MLDs adopt identical backoff parameters, SB-MLDs demonstrate superior performance in both data rate and mean access delay, particularly in scenarios with a large number of links, indicating a severe fairness issue in multi-link WiFi 7 networks with dual channel access schemes.

With a target ratio of data rates between LB-MLDs and SB-MLDs, we further develop an adaptive backoff parameter tuning strategy for optimizing the sum rate and access delay performance. Specifically, as the network size increases, the initial backoff window sizes of both LB-MLDs and SB-MLDs should be linearly incremented. Moreover, as the number of links grows, LB-MLDs should diminish their initial backoff window size while SB-MLDs should escalate theirs; As the target ratio increases, the initial backoff window size of LB-MLDs should be declined while that of SB-MLDs should be enlarged. The corresponding maximum network sum rate and minimum mean access delay are both derived.

Our analysis offers valuable insights for the practical design of multi-link WiFi 7 networks. It is demonstrated that using fixed initial backoff window sizes leads to substantial performance degradation as the network size increases, along with the potential for significant unfairness between LB-MLDs and SB-MLDs. However, by employing the optimal setting, it is possible to consistently achieve the maximum network sum rate and the target ratio of device data rates, irrespective of variations in the network size.

Note that although this paper focuses on the non-STR mode, the analysis can further be extended to study the STR mode where each interface of an MLD performs the channel access procedure and makes transmission attempts independently, based on which comparison between non-STR and STR modes can further be made. In addition, a key assumption in this paper is no decoding errors due to noise and fading, the performance optimization of multi-link IEEE 802.11be WiFi 7 network with more practical channel models is another interesting issue that deserves much attention in the future

study.

APPENDIX A DERIVATION OF (6) AND (7)

Since an HOL packet must wait for a number of idle slots equal to the value of the *shared backoff counter* before it can be transmitted, we have

$$r_i^{(\phi)} = \frac{1}{1 + E[b_i^{(\phi)}]}, \quad (46)$$

$\phi = LB, SB$, where $E[b_i^{(\phi)}]$ is the average value of the initial *shared backoff counter* when an HOL packet of Type ϕ enters State R_i .

Let $\beta_{i,j}^{(\phi)}$, $\phi = LB, SB$ represent the probability of the *shared backoff counter* being j upon entering State R_i . In the case of LB, a *shared backoff counter* value of j implies that all values are no larger than j , but cannot be all smaller than j . Therefore, $\beta_{i,j}^{(LB)}$ can be expressed as

$$\beta_{i,j}^{(LB)} = \left(\frac{j+1}{W_i^{(LB)}} \right)^M - \left(\frac{j}{W_i^{(LB)}} \right)^M. \quad (47)$$

In a similar manner, if the backoff counters have a minimum value of j , it implies that all the counters are at least j , but not all of them are strictly greater than j . Consequently, $\beta_{i,j}^{(SB)}$ can be determined as

$$\beta_{i,j}^{(SB)} = \left(\frac{W_i^{(SB)} - j}{W_i^{(SB)}} \right)^M - \left(\frac{W_i^{(SB)} - (j+1)}{W_i^{(SB)}} \right)^M. \quad (48)$$

Given (47), we have

$$\begin{aligned} E[b_i^{(LB)}] &= \sum_{j=0}^{W_i^{(LB)}-1} j \beta_{i,j}^{(LB)} = \frac{1}{(W_i^{(LB)})^M} \cdot \sum_{j=0}^{W_i^{(LB)}-1} j ((j+1)^M - j^M) \\ &= \frac{1}{(W_i^{(LB)})^M} \cdot \left(\sum_{j=0}^{W_i^{(LB)}-1} ((j+1)^{M+1} - j^{M+1}) - \sum_{j=0}^{W_i^{(LB)}-1} (j+1)^M \right) \\ &= \frac{1}{(W_i^{(LB)})^M} \cdot \left((W_i^{(LB)})^{M+1} - \sum_{j=1}^{W_i^{(LB)}} j^M \right). \end{aligned} \quad (49)$$

We further have

$$\begin{aligned} \sum_{j=1}^{W_i^{(LB)}} j^M &= \frac{(W_i^{(LB)})^{M+1}}{M+1} + \frac{1}{2} (W_i^{(LB)})^M \\ &\quad + \sum_{k=2}^M \frac{B_k}{k!} \frac{M!}{(M-k+1)!} (W_i^{(LB)})^{M-k+1}, \end{aligned} \quad (50)$$

where $\{B_k\}$, $k = 2, \dots, M$ are Bernoulli numbers, by following Faulhaber's formula [23]. For a large $W_i^{(LB)}$, the third term in (50) is much smaller than $(W_i^{(LB)})^M$, and can be ignored, then by combining (46) and (49)-(50), (6) can be obtained.

Similarly, for SB, we have

$$\begin{aligned} E[b_i^{(SB)}] &= \frac{1}{(W_i^{(SB)})^M} \cdot \left(\sum_{j=0}^{W_i^{(SB)}-1} (j(W_i^{(SB)} - j))^M \right. \\ &\quad \left. - (j+1)(W_i^{(SB)} - (j+1))^M \right) + \sum_{j=0}^{W_i^{(SB)}-1} (W_i^{(SB)} - (j+1))^M \\ &= \frac{1}{(W_i^{(SB)})^M} \cdot \sum_{j=0}^{W_i^{(SB)}-1} (W_i^{(SB)} - (j+1))^M = \frac{1}{(W_i^{(SB)})^M} \cdot \sum_{j=0}^{W_i^{(SB)}-1} j^M \\ &\approx \frac{W_i^{(SB)}}{M+1} - \frac{1}{2}. \end{aligned} \quad (51)$$

By substituting (51) into (46), (7) can be obtained.

APPENDIX B DERIVATION OF (9)

By following the Bayes' rule, we have

$$\begin{aligned} \alpha_{R_i}^{(\phi)} &= \Pr\{\text{channel is idle} \mid \text{the HOL packet is in State } R_i\} \\ &= \frac{\alpha \Pr\{\text{the HOL packet is in State } R_i \mid \text{channel is idle}\}}{\Pr\{\text{the HOL packet is in State } R_i\}}. \end{aligned} \quad (52)$$

Note that when the channel is idle, the HOL packet must be in State R_k , $k = 0, 1, \dots, K$. Therefore, (52) can be further written as

$$\begin{aligned} \alpha_{R_i}^{(\phi)} &= \alpha \cdot \frac{\tilde{\pi}_{R_i}^{(\phi)}}{\sum_{k=0}^K \tilde{\pi}_{R_k}^{(\phi)}} = \frac{\alpha}{\sum_{k=0}^K \tilde{\pi}_{R_k}^{(\phi)}} \\ &= \frac{\alpha}{1 - (\tilde{\pi}_T^{(\phi)} + \sum_{k=0}^K \tilde{\pi}_{F_k}^{(\phi)})}. \end{aligned} \quad (53)$$

(9) can then be obtained by combining (1)-(3) and (53).

APPENDIX C DERIVATION OF (16)

Let $\omega^{(\phi)}$ denote the probability that an MLD of Type $\phi = LB, SB$ transmits a packet when the channel is idle. We have

$$\begin{aligned} \omega^{(\phi)} &= \Pr\{\text{MLD of Type } \phi \text{ transmit} \mid \text{channel is idle}\} \\ &= \frac{\sum_{i=0}^K \tilde{\pi}_{R_i}^{(\phi)} r_i^{(\phi)}}{\sum_{i=0}^K \tilde{\pi}_{R_i}^{(\phi)}}. \end{aligned} \quad (54)$$

By substituting (8) into (54), we further have

$$\omega^{(\phi)} = \frac{\sum_{i=0}^K \frac{\tilde{\pi}_{R_i}^{(\phi)}}{\tau_{R_i}^{(\phi)}}}{\alpha_{R_i}^{(\phi)} \sum_{i=0}^K \tilde{\pi}_{R_i}^{(\phi)}}. \quad (55)$$

According to (1) and (2), it can be obtained that

$$\tilde{\pi}_{R_i}^{(\phi)} = \frac{\pi_{R_i}^{(\phi)} \tau_{R_i}^{(\phi)}}{\pi_T^{(\phi)} \tau_T} \tilde{\pi}_T^{(\phi)} \quad \text{and} \quad \sum_{i=0}^K \pi_{R_i}^{(\phi)} = \frac{\pi_T^{(\phi)}}{p}. \quad (56)$$

By substituting (56) into (55), we further have

$$\omega^{(\phi)} = \frac{\tilde{\pi}_T^{(\phi)}}{p \tau_T \alpha_{R_i}^{(\phi)} \sum_{i=0}^K \tilde{\pi}_{R_i}^{(\phi)}}. \quad (57)$$

By combining (53) and (57), the probability that an MLD of Type $\phi = LB, SB$ transmits a packet when the channel is idle, $\omega^{(\phi)}$, can be derived as

$$\omega^{(\phi)} = \frac{\tilde{\pi}_T^{(\phi)}}{p\tau_T\alpha}, \quad (58)$$

with which (16) can further be obtained.

REFERENCES

- [1] C. Deng, X. Fang, X. Han, X. Wang, L. Yan, R. He, Y. Long, and Y. Guo, "IEEE 802.11be Wi-Fi 7: New Challenges and Opportunities," *IEEE Commun. Surv. Tutorials*, vol. 22, no. 4, pp. 2136–2166, 4th Quart. 2020.
- [2] A. López-Raventós and B. Bellalta, "Multi-Link Operation in IEEE 802.11be WLANs," *IEEE Wireless Commun.*, vol. 29, no. 4, pp. 94–100, Aug. 2022.
- [3] I. Jang, J. Choi, J. Kim, S. Kim, S. Park, and T. Song, "Channel Access for Multi-Link Operation," document IEEE 802.11-19/1144r6, Nov. 2019.
- [4] S. Naribole, S. Kandala, W. B. Lee, and A. Ranganath, "Multi-Link Channel Access Discussion," document IEEE 802.11-19/1405r7, Nov. 2019.
- [5] Y. Seok, D. Akhmetov, D. Ho, R. Chitrakar, M. Gan, I. Jang, and S. Naribole, "UL Sync Channel Access Procedure," document IEEE 802.11-20/1730r3, Nov. 2020.
- [6] Y. Li, Y. Guo, G. Huang, Y. Zhou, M. Gan, and D. Liang, "Channel Access in Multi-Band Operation," document IEEE 802.11-19/1116r5, Sep. 2019.
- [7] *IEEE Draft Standard for Information technology–Telecommunications and information exchange between systems Local and metropolitan area networks–Specific requirements - Part 11: Wireless LAN Medium Access Control (MAC) and Physical Layer (PHY) Specifications Amendment: Enhancements for Extremely High Throughput (EHT)*, IEEE Std 802.11be/D5.0, 2023.
- [8] S. Naribole, W. B. Lee, S. Kandala, and A. Ranganath, "Simultaneous Transmit-Receive Multi-Channel Operation in Next Generation WLANs," in *Proc. IEEE WCNC*, 2020, pp. 1–8.
- [9] G. Naik, D. Ogbe, and J. Park, "Can Wi-Fi 7 Support Real-Time Applications? On the Impact of Multi Link Aggregation on Latency," in *Proc. IEEE ICC*, 2021, pp. 1–6.
- [10] S. Naribole, S. Kandala, and A. Ranganath, "Multi-Channel Mobile Access Point in Next-Generation IEEE 802.11be WLANs," in *Proc. IEEE ICC*, 2021, pp. 1–7.
- [11] M. Alsakati, C. Pettersson, S. Max, V. N. Moothedath, and J. Gross, "Performance of 802.11be Wi-Fi 7 with Multi-Link Operation on AR Applications," in *Proc. IEEE WCNC*, 2023, pp. 1–6.
- [12] G. Bianchi, "Performance Analysis of the IEEE 802.11 Distributed Coordination Function," *IEEE J. Sel. Areas Commun.*, vol. 18, no. 3, pp. 535–547, Mar. 2000.
- [13] T. Song and T. Kim, "Performance Analysis of Synchronous Multi-Radio Multi-Link MAC Protocols in IEEE 802.11be Extremely High Throughput WLANs," *Appl. Sci.*, vol. 11, no. 1, pp. 1–27, Dec. 2020.
- [14] T. Jin, J. Guo, L. Lin, Y. Wang, and Y. Chen, "Performance Analysis of Synchronous Multilink MAC Protocol with Automatic Repeat Request," *Mob. Inf. Syst.*, vol. 2022, no. 4049008, pp. 1–11, Sep. 2022.
- [15] N. Korolev, I. Levitsky, and E. Khorov, "Analytical Model of Multi-Link Operation in Saturated Heterogeneous Wi-Fi 7 Networks," *IEEE Wireless Commun. Lett.*, vol. 11, no. 12, pp. 2546–2549, Dec. 2022.
- [16] B. Bellalta, M. Carrascosa, L. Galati-Giordano, and G. Geraci, "Delay Analysis of IEEE 802.11be Multi-link Operation under Finite Load," *IEEE Wireless Commun. Lett.*, vol. 12, no. 4, pp. 595–599, Apr. 2023.
- [17] L. Dai and X. Sun, "A Unified Analysis of IEEE 802.11 DCF Networks: Stability, Throughput, and Delay," *IEEE Trans. Mobile Comput.*, vol. 12, no. 8, pp. 1558–1572, Aug. 2013.
- [18] Y. Gao, X. Sun, and L. Dai, "Throughput Optimization of Heterogeneous IEEE 802.11 DCF Networks," *IEEE Trans. Wireless Commun.*, vol. 12, no. 1, pp. 398–411, Jan. 2013.
- [19] —, "IEEE 802.11e EDCA Networks: Modeling, Differentiation and Optimization," *IEEE Trans. Wireless Commun.*, vol. 13, no. 7, pp. 3863–3879, July 2014.
- [20] Y. Gao and S. Roy, "Achieving Proportional Fairness for LTE-LAA and Wi-Fi Coexistence in Unlicensed Spectrum," *IEEE Trans. Wireless Commun.*, vol. 19, no. 5, pp. 3390–3404, May 2020.
- [21] W. Zhan, B. Wu, X. Sun, K. Xie, and X. Chen, "Fairness-Constrained Rate Optimization of Multi-Link Slotted Aloha," *IEEE Networking Lett.*, vol. 5, no. 1, pp. 31–35, Mar. 2023.
- [22] R. M. Corless, G. H. Gonnet, D. E. G. Hare, D. J. Jeffrey, and D. E. Knuth, "On the Lambert W Function," *Adv. Comput. Math.*, vol. 5, pp. 329–359, Dec. 1996.
- [23] D. E. Knuth, "Johann Faulhaber and Sums of Powers," *Math. Comput.*, vol. 61, pp. 277–294, July 1993.